Electronic Transport in Dye-Sensitized Nanoporous TiO_2 Solar Cells—Comparison of Electrolyte and Solid-State Devices

G. Kron, T. Egerter, J. H. Werner, and U. Rau*

Institute of Physical Electronics, University of Stuttgart, 70569 Stuttgart, Germany

Received: October 17, 2002

This article compares the electronic transport properties of dye-sensitized solar cells using a liquid electrolyte with those of one using an organic hole conductor. Both types of solar cells differ by the reference energies for recombination and, in particular, by their recombination probabilities of photoinjected electrons from the titanium dioxide into the respective contact medium. For voltages below 0.8 V, the junction impedance of the electrolyte cell is dominated by diffusion and recombination of electrons from the TiO_2 into the electrolyte. The impedance of the solid state exhibits a negative reactance, that is, an inductive behavior, which we attribute to conductivity modulation of the hole conductor by injected electrons.

I. Introduction

Photoelectrochemical solar cells based on dye-sensitized nanocrystalline TiO_2[1,2] have attracted considerable interest because of their demonstrated power conversion efficiencies, η, with $\eta > 10\%$ obtained from laboratory cells,[3] as well as by their simple preparation technology and their potential low cost. The dye-sensitized solar cell (DSSC) is built up by an approximately 10 μm thick layer of nanoporous sponge-type TiO_2 deposited and sintered onto a SnO_2/F-covered glass substrate. The TiO_2 nanoparticles are covered with a monolayer of dye molecules. Photoexcitation of the dye and the transfer of the electron from the excited state into the conduction band of the TiO_2 make up the primary photovoltaic action of the device.[2] The oxidized dye molecule is reduced by the I^-/I_3^- redox couple of the electrolyte (EL) in contact with the TiO_2 grain. A Pt back electrode serves for the reduction of the I_3^- ion, whereas the photoelectron diffuses through the network of TiO_2 particles toward the SnO_2/F front electrode.

One critical feature of the DSSC is the liquid electrolyte containing the I^-/I_3^- redox couple in a highly volatile solvent. The liquid phase often causes leakage and makes cell encapsulation and cell interconnections within modules rather difficult.[4] Replacing the liquid electrolyte by a solid-state medium seems to be a solution for these problems.[4] Several attempts have been made to find a suitable material, mostly an organic polymer or nonpolymer, hole conductor (HC).[5−7] In the case of the solid-state DSSC, electrons from the highest occupied molecular orbital (HOMO) of the hole conductor regenerate the dye molecules instead of the redox couple of the electrolyte. Thus, the primary photovoltaic action generates an electron in the TiO_2 and a hole in the HC. The basic feasibility of such a modified charge transfer was demonstrated in refs 5−7. However, in none of these cases can the achieved power conversion efficiencies ($\eta < 2\%$) compete with the $\eta > 10\%$ of the original electrolyte DSSC. Open-circuit voltages, V_{oc}, of the solid-state DSSC are $V_{oc} \approx 400-500$ mV (compared to $V_{oc} \approx 800$ mV of the electrolyte devices) and short-circuit current densities, J_{sc}, are $J_{sc} = 3$ mA cm^{-2} (compared to $J_{sc} = 20$ mA cm^{-2} for devices with electrolyte). Thus, both photovoltaic output parameters of the solid-state DSSC lack behind those of its liquid-based counterpart.

This paper presents a comparative study of the electronic transport properties of both the electrolyte and the solid-state DSSC, by means of direct current (dc) and alternating current (ac) measurements. The open-circuit voltage, V_{oc}, of the solid-state DSSC is lower than the V_{oc} of the electrolyte-based counterpart for two reasons: (i) the less favorable equilibrium Fermi-level position in the TiO_2 and (ii) because of the much larger recombination probability of photogenerated electrons from the TiO_2 with holes in the HC as compared to recombination with the I^-/I_3^- redox couple.[8] Investigation of the impedance of both types of devices unveils that the basic features of the ac transport properties are understood with the concepts of a classical pn-heterojunction device. The low-frequency capacitance of the electrolyte DSSC exhibits an exponential increase upon application of a forward voltage similarly to the diffusion capacitance of a pn-junction diode.[9] Under the same conditions, the impedance of the solid-state device exhibits a negative reactance, that is, an inductance, which results from conductivity modulation in the HC induced by the electrons injected from the SnO_2/F contact into the TiO_2 network. Such inductive behavior is, again, known from pn-junctions under high injection conditions.[10]

II. Basics

Equilibrium Band Diagram. Here, we discuss the working principles of the original electrolyte DSSC with a special focus on possible modifications that might arise by substituting the electrolyte by a HC. Despite of the ongoing discussion on the nature of photovoltaic action and the limitations on the performance of the original cell, there is at least an agreement on the primary process of charge separation upon illumination. The basic action relies on photoexcitation of the dye, the subsequent injection of the excited electron in the TiO_2, and the regeneration of the dye via the I^-/I_3^- redox couple. Electron injection into the TiO_2 takes place on an ultrafast time scale

* To whom correspondence should be addressed. Address: Institute of Physical Electronics (*ipe*), University Stuttgart, Pfaffenwaldring 47, 70569 Stuttgart, Germany. Phone: +49 711 6857199. Fax: +49 711 6857143. E-mail: uwe.rau@ipe.uni-stuttgart.de.

10.1021/jp0222144 CCC: $25.00
Published on Web 03/26/2003

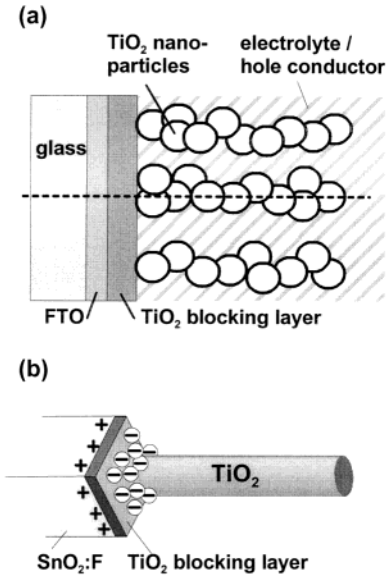

Figure 1. Schematic cross section (a) of the dye-sensitized nanocrystalline solar cell and (b) balance of the Fermi levels of SnO_2/F and electrolyte leading to positive space charge in the SnO_2/F. The negative charge (anions) of the electrolyte approaches the SnO_2/F layer as close as possible at the bottom of the spongelike TiO_2 structure.

below 10^{-12} s.[11−13] Regeneration of the dye by an electron from the redox couple takes place within a time of 10 ns.[14]

Despite the complication by the nanoscale mixture of TiO_2 and electrolyte, the energy-band diagram of the electrolyte DSSC in thermal equilibrium is fairly well understood. Here, it is helpful to idealize the TiO_2 network as columns with a diameter of 10−15 nm placed on the SnO_2/F (as in the electrolyte DSSC) or on an additional amorphous TiO_2 blocking layer (as in the solid-state DSSC). These columns are immersed into the electrolyte or HC as shown in Figure 1a. Because the TiO_2 is only moderately doped, the charge within individual TiO_2 particles is too small to provide a band bending *across* the grain in excess of a few millielectronvolts.[15] Furthermore, even this small charge in the colloids is screened by the Helmholtz layer of the electrolyte such that also *along* the TiO_2 columns there is no considerable electrical field. The resulting band diagram for the conduction and valence band energies, E_c and E_v, in the center of a TiO_2 column immersed in the electrolyte is shown in Figure 2a.

The position of the equilibrium Fermi level, E_F, at the TiO_2−electrolyte interface is determined by the Fermi level (i.e., the redox energy, E_{redox}) of the electrolyte.[16] In addition, an interface dipole exists at the TiO_2/EL interface as indicated in the vacuum level, E_{vac}, in Figure 2a, resulting from the polarity of the adsorbed dye, from the Helmholtz layer of the electrolyte, and from the adsorption of the Li^+ cations, which come closer to the interface than the I^- anions.[17,18] Thus, the arrangement of charged species close to the TiO_2/EL interface provides a potential drop V_{if} that shifts the conduction band energy of the TiO_2 downward with respect to E_{redox} of the electrolyte.

To arrange the Fermi energies at the TiO_2−SnO_2/F interface requires an additional voltage drop, V_{bi}, close to this interface. From Figure 2a, we find

$$qV_{bi} = E_{vac} - E_{redox} - \chi_{SnO_2} - qV_{if} \qquad (1)$$

where χ_{SnO_2} denotes the electron affinity of the SnO_2/F. Note that the potential V_{if} drops over the TiO_2−electrolyte interface everywhere along the TiO_2 column. Because of the similarity

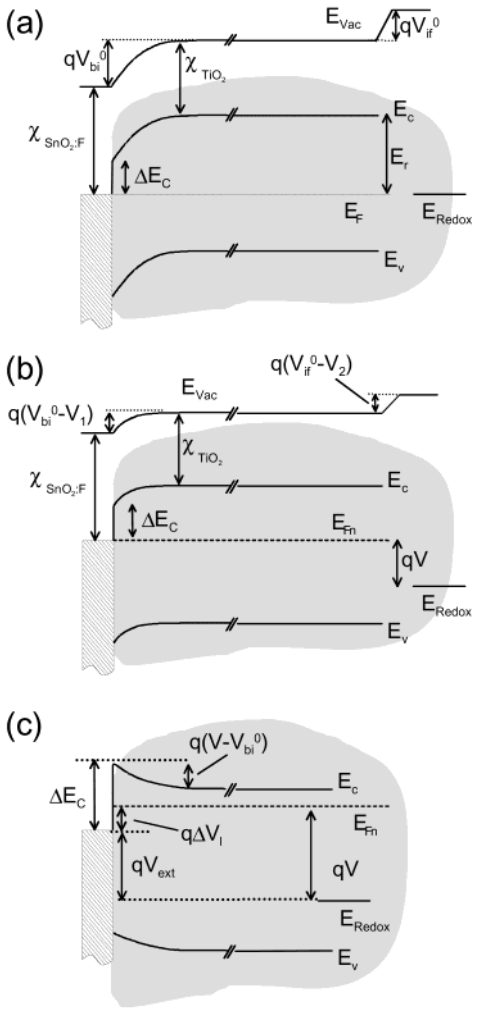

Figure 2. Band model of the dye sensitized solar cell (a) in the dark and (b) under illumination. The band bending at the TiO_2−SnO_2/F interface is due to negative charges inside the electrolyte. The built-in voltage is reduced by the photovoltage, V, to $V_{bi} = V_{bi}^0 - V$. Panel c shows detail of the band diagram in a situation in which the light-induced (internal) voltage, V, exceeds the built-in voltage, V_{bi}^0. Here, a barrier, $V - V_{bi}^0$, builds up at the TiO_2−SnO_2/F interface such that under working conditions of the solar cell a loss voltage, ΔV_l, might diminish the external voltage, V_{ext}, available at the contacts.

of the band diagram in Figure 2a with that of a regular bulk heterojunction,[19] we denote the potential drop across the TiO_2−SnO_2/F interface as a built-in voltage, V_{bi}. The difference between a bulk heterojunction and the DSSC in that respect is, however, that V_{bi} is built up by *negative charges in the electrolyte* penetrating the nanoporous TiO_2 network as shown in Figure 1b. The respective positive charges, resulting from the ionized donor atoms of the highly doped SnO_2/F, are situated in a very thin layer close to the TiO_2 interface. Because of the geometrical arrangement of the charges around the TiO_2 columns, the built-in field cannot penetrate much deeper into the TiO_2 than the diameter of the column.[19−21] Thus, the built-in voltage only affects the first one or two TiO_2 nanograins of the column. Because of the low charge density in the TiO_2, no quantity concerning the TiO_2 enters in eq 1. Cahen and coworkers[16] estimated the built-in voltage in a standard DSSC to $V_{bi} \approx 0.3$ V, whereas Schwarzburg and Willig give a value of $V_{bi} \approx 0.7$ V.[19]

The question of the magnitude and importance of the built-in voltage in the DSSC is still controversially discussed.[16−19,21,22] Here, it is important to state that this question should not be

mixed up with another question, namely, the question whether the DSSC can be treated in analogy to a classical pn-(hetero)-junction solar cell. We will show in the following that a treatment of the DSSC with the tools provided by Shockley's theory of pn-junctions[9] carries us relatively far in the analysis and understanding of both devices, the EL−DSSC, as well as the HC−DSSC. However, we *do not* conclude from our experimental findings that the built-in voltage sets an upper limit for the open-circuit voltage of the DSSC as this is also not necessarily the case for pn-junction solar cells.

Band Diagram under Illumination. Upon illumination of the solar cell, the number of electrons in the TiO_2 increases by injection of photoelectrons from the dye, and thus, the Fermi-level splits up into that for electrons (in the TiO_2) and that in the electrolyte. This is the primary photovoltaic action of the DSSC. However, to measure an external photovoltage, we need to couple the excess electrons of the TiO_2 to the SnO_2/F front electrode and the redox potential of the redox couple to the Pt back electrode.

At open circuit, the photogeneration current density, j_{ph}, equals the recombination current density, j_r. Because of the large effective interface area between the TiO_2 and the electrolyte/HC, the most likely recombination path for photoelectrons in the TiO_2 is interface recombination with the oxidized species of the redox couple; in case of the solid-state DSSC, the electrons recombine with a hole from the HOMO. This basic situation was considered by Cahen and co-workers.[16] These authors identified V_{oc} with $\Delta\mu$ at $j_r = j_{ph}$, $\Delta\mu$ being the difference between the chemical potentials of the electrons in the TiO_2 under illumination and in equilibrium.

According to Gerischer's semiconductor−electrolyte electron transfer theory,[23] a general expression for V_{oc} was derived[24,25] as

$$V_{oc} = \frac{kT}{q}\ln\left\{\frac{j_{ph}}{q\upsilon(E_c)\left(\frac{kT}{4\pi\lambda}\right)^{1/2}N_c c_{ox}}\right\} + \frac{E_c - E_{redox}}{q} + \frac{(E_c - E^0 - \lambda)^2}{4\lambda q} \quad (2a)$$

Here, N_c is the effective density of states in the conduction band, c_{ox} is the concentration of oxidized species in the electrolyte, and $\upsilon(E_c)$ represents the frequency factor for the electron transfer from the semiconductor into the electrolyte at the energy of the conduction band edge, E_c.[26] The quantity E^0 denotes the standard redox potential in Nernst's equation for the redox potential of the electrolyte, and λ denotes the solvation reorganization energy. The prerequisite for eq 2a is that the number of excess charge carriers (electrons) at the TiO_2−EL interface is controlled by the externally applied voltage, regardless whether that voltage drops over a space charge region in the TiO_2 or over the SnO_2/F−TiO_2 interface. With the same precondition, the open-circuit voltage, V_{oc}, of the solid-state device is limited by recombination of photogenerated electrons (in the TiO_2) with holes (in the HC),[27] according to

$$V_{oc} = \frac{kT}{q}\ln\left\{\frac{j_{ph}}{qSN_c}\right\} + \frac{E_c - E_F}{q} \quad (2b)$$

In eq 2b, the quantity N_c is the effective density of states in the conduction band of the TiO_2 and S is the interface recombination velocity.

External Voltage. Any voltage drop over the device implies that the effective band diagram in Figure 2a has to be modified as shown in Figure 2b. If we consider only the two potential barriers, V_{bi} and V_{if}, an externally measured or externally applied voltage, $V = V_1 + V_2$, causes either one or both of these quantities to be reduced according to

$$V_{bi} + V_{if} = V_{bi}^0 - V_1 + V_{if}^0 - V_2 = V_{bi}^0 + V_{if}^0 - V \quad (3)$$

Here, it holds that $V_{bi}^0 = V_{bi}$ ($V = 0$), $V_{if}^0 = V_{if}$ ($V = 0$), and V_1 and V_2 are as defined in Figure 2b. The decrease of the built-in voltage, V_{bi}, by an applied voltage bias resembles the reduction of the built-in potential in a bulk pn-junction diode, whereas a decrease of V_{if} has no analogue in such a device.

As mentioned by Zaban an co-workers,[17] an exclusive drop of the external voltage, V, over the TiO_2−EL interface, that is, a reduction of V_{if}^0 by $V = V_2$ and $V_1 = 0$, would lead to an internal barrier, hindering electron injection into the TiO_2 or dye regeneration from the electrolyte or both. If the external voltage, V, only affected the built-in voltage, V_{bi}, one might ask the question what happens if the voltage V significantly exceeds the built-in voltage, V_{bi}^0. In such a situation, photoelectrons from the TiO_2 would have to overcome a significant potential barrier between the TiO_2 and the SnO_2/F window layer. Such a barrier does not necessarily affect the open-circuit voltage but would lead to resistive losses, which at the end would degrade the fill factor. Recent two-dimensional numerical simulations of DSSC by Ferber and Luther[21] show that built-in voltages as low as 0.48 V allow for an open-circuit voltage around 0.78 V. This theoretical finding is not in contradiction to the assumptions outlined above because the upper V_{oc} limit imposed by eq 2a or 2b, as well as by Figure 2a,b, is given by $V_{oc} < V_{bi}^0 + \Delta E_c$, $\Delta E_c = \chi_{SnO_2} - \chi_{TiO_2}$. However, Figure 9 in ref 21 indicates that the fill factor of the illuminated current (I)/voltage (V) curves starts to degrade when turning from $V_{bi}^0 = 0.66$ to 0.48 V. As sketched in Figure 2c, the loss of fill factor is due to a loss-voltage, ΔV_l, that is needed to drive the electrons from the TiO_2 over the electrostatic barrier of height $V - V_{bi}^0$ into the SnO_2/F window layer. The voltage V_{ext} that can be used at the outer electrodes, then, is reduced to $V_{ext} = V - \Delta V_l$, where here V denotes the internal voltage due to the light-induced shift of the electron Fermi level in the TiO_2. As shown more explicitly in section V, the magnitude of ΔV_l depends on the actual current flow over the TiO_2−SnO_2/F interface and is zero at $V_{ext} = V = V_{oc}$.

The purpose of the capacitance measurements in the ac part of section IV is to decide whether an external applied voltage drops over the SnO_2/F−TiO_2 or the TiO_2−electrolyte interface. In the first case, one would expect to measure an exponentially increasing diffusion capacitance like that in bulk pn-junction diodes,[9] whereas the second case would give us the capacitance of the Helmholtz layer around all nanoparticles.

Diffusive Carrier Transport. Because of the absence of an electrical field in the major part of the TiO_2 network, transport of electrons toward the front electrode, under illumination (or under forward bias), from the front electrode into the TiO_2 nanoparticles occurs by diffusion. Within the range of working condition, that is, at moderate forward bias $V < V_{oc}$, we would expect the admittance of the DSSC to be dominated by the diffusion admittance of the electrons in the TiO_2. As given by Shockley[9] for classical (single-sided) pn-junctions, the solution for the time-dependent diffusion equation leads to the complex diffusion admittance, Y_{diff}, of minority carriers for $V > 3kT/q$

$$Y_{diff} = \frac{qn_j D_e}{L_{De}^*}\frac{q}{kT}\tanh\frac{d_T}{L_{De}^*} \quad (4)$$

where D_e is the diffusion constant, n_j is the excess electron density, $n_j = n_0(\exp(qV/(kT)) - 1)$, n_0 being the equilibrium electron density, and $L^*_{De} = L_{De}(1 + i\omega\tau)^{-1/2}$, L_{De} being the effective diffusion length, a complex value that depends on the angular frequency, $\omega = 2\pi f$. Note that eq 4 neglects recombination at the end of the TiO_2 column of length, d_T.

Solid-State DSSC. The band model in Figure 2a,b is developed for the DSSC using a liquid electrolyte. For the case of the solid-state DSSC, we have to take two main differences into consideration. First, the Fermi energy level of the organic hole conductor is different from the redox niveau of the I^-/I_3^- redox couple ($E_{vac} - E_{redox} = -4.95$ eV,[28]). The Fermi energy in the solid-state cell depends on effective density of states in the valence band (HOMO), N_V, and on the doping density according to

$$E_F = E_{HOMO} + kT \ln\left(\frac{N_V}{N_A}\right) \tag{5}$$

Using $N_V \approx 10^{21}$ cm^{-3} [29] and $N_A \approx 10^{17}$ cm^{-3} (cf. ac part of section IV), we calculate that the Fermi energy, E_F, in the HC is 0.24 eV above the energy E_{HOMO} of the HOMO. The latter energy was measured by cyclovoltammetry to approximately $E_{HOMO} - E_{vac} = -4.8$ eV for the HC in solution. Although the solid-state value for the position of the HOMO of the HC might differ slightly, we estimate from the above assumption a difference of 0.2 eV between E_{HOMO} in the solid-state cell and the redox energy in the electrolyte cell. The other main difference between solid-state and electrolyte DSSC lies in the lower charge carrier density of the hole conductor, in contrast to the high ion density of the redox electrolyte. Thus, the very thin Helmholtz layer is replaced by a much wider space charge region.

III. Sample Preparation

The preparation of the solar cells starts with a glass substrate, deposited by SnO_2/F as transparent conducting oxide (TCO). We clean the substrate in an ultrasonic bath using Helmanex, pure water, and 2-propanol. Following ref 30, we subsequently deposit a thin TiO_2 blocking layer on top of the TCO by a spray pyrolysis process using a 0.2 M dipropoxy titanium bis-(acetylacetonate) solution in ethanol. After tempering the blocking layer at 500 °C for 1 h, we deposit the nanoporous TiO_2 film by screen printing of a TiO_2 paste (Titan-Nanoxid TSP) of Solaronix. The TiO_2 is then sintered on a hotplate at 450 °C for 30 min. The monolayer of the dye is deposited by dipping the samples for 8 h into a dye solution after cooling to approximately 100 °C. For preparation of the dye solution, we take the standard dye $RuL_2(NCS)_2$, normally referred to as N3 dye, with a concentration of 5×10^{-4} M in ethanol.

Standard electrolyte DSSCs are completed by dripping a small amount of Solaronix Iodolyte TG 50 on the dye layer and contacting it with a Pt back electrode. For the preparation of solid-state DSSC, we use the organic hole transport material 2,2′,7,7′-tetrakis(*N*,*N*-di-*p*-methoxyphenyl amine)-9,9′-spirobifluorene (MeO-spiro-TAD)[31,32] dissolved in chlorobenzene together with tribromophenylammonium hexachloroantimonate as dopand and additional lithium salt, $Li((CF_3SO_2)_2N)$. The 0.17 M solution is spin-coated on the dye-covered porous surface of the TiO_2 and finally back-contacted by an evaporated Au electrode.

For the dc-characterization of the solar cells, we measure *IV* characteristics with a Keithley source-measure unit, model 2400. For temperature-dependent *IV* measurements, the samples are placed in a cryostat that is cooled with liquid nitrogen. For ac-characterization (admittance spectroscopy), we use an EG&G 273A potentiostate and a Solartron 1250 frequency response analyzer (FRA). The potentiostate keeps an applied voltage between front and back electrode constant, while the FRA takes over the main measurement, excitation, and analysis of the system's response. All ac and dc measurements are performed in air, limiting the available range of temperatures to 280 K and above.

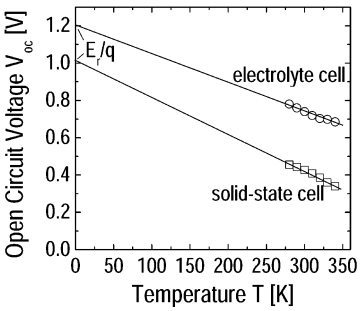

Figure 3. Open-circuit voltage, V_{oc}, versus temperature, T, for the electrolyte and the solid-state DSSC. The y-axis intercept yields the reference energy, E_r. The steeper slope of the V_{oc} vs T in case of the solid-state DSSC indicates a higher recombination probability in this device.

IV. Electrical Characterization

dc Characterization. In this section, we determine the reference energy, E_r, for the recombination process dominating the open-circuit voltage. The value is extracted from temperature-dependent *I/V* characteristics under illumination as shown in Figure 3. The quantity E_r indicates the reference energy of the solar cell, which gives a hypothetical maximum $V_{oc,max}$ by division with the elementary charge q at temperature $T = 0$ K. In Figure 2a, E_r is shown as difference between the TiO_2 conduction band energy, E_c, and the equilibrium Fermi level, E_F. As can be seen from eq 2a, V_{oc} has an almost linear dependence on temperature. The y-axis intercept of eq 2a gives

$$y(T{=}0\text{K}) = \frac{E_c - E_{redox}}{q} + \frac{(E_c - E^0 - \lambda)^2}{4\lambda q} \tag{6a}$$

The y-axis intercept of eq 2b has to account for the temperature dependence of the Fermi energy (eq 5) and therefore reads

$$y(T{=}0\text{K}) = \frac{E_c - E_{HOMO}}{q} \tag{6b}$$

Thus, we define the differences $E_c - E_{redox}$ in eq 6a and $E_c - E_{HOMO}$ in eq 6b as the reference energies of the respective recombination processes. These reference energies correspond to the maximum attainable V_{oc}, namely, the (extrapolated) value V_{oc} ($T = 0$ K).

The experimental data are shown in Figure 3. Note that our current/voltage measurements are limited to a temperature range $T > 280$ K because for both devices the experiments had to be performed in air. From the V_{oc} data in the temperature range $350 \geq T \geq 280$ K in Figure 3, we extrapolate maximum open-circuit voltages at $T = 0$ K of $V^{solid}_{oc,max} \approx 1.0$ V for the solid state and $V^{electrolyte}_{oc,max} \approx 1.2$ V for the electrolyte device. The value of λ in eq 2a, valid for the EL device, is generally in the range 0.5−2 eV, depending on the interaction of the redox molecule with the solvent.[33] Considering the extrapolated V_{oc} values, we neglect the second term in eq 6a for the y-axis intercept and

get the reference energies $E_r^{solid} \approx 1$ eV and $E_r^{electrolyte} \approx 1.2$ eV. Thus, the reference energies, E_r, differ by about 0.2 eV for the two types of solar cells. The determination of the reference energy in Figure 3 requires extrapolation over a wide temperature range. In addition, E_{redox} is temperature-dependent according to Nernst's equation for the redox potential of electrolytes, $E_{redox} = E^0 + kT \ln(c_{ox}/c_{red})$, which yields a difference in E_{redox} of approximately 0.06 eV for the extrapolated temperature range. Therefore, the reference energies, $E_r^{electrolyte}$ and E_r^{solid}, as well as the difference $\Delta E_r = E_r^{electrolyte} - E_r^{solid}$, are subject to considerable error bars (± 0.1 eV). However, the experimental result of the difference in reference energies $\Delta E_r \approx 0.2$ eV fits well to the estimated difference of 0.2 eV between E_{redox} and the position of the HOMO of the HC in section II.

The difference between the open-circuit voltages of the electrolyte and the solid-state DSSC, ΔV_{oc}, amounts to 0.4−0.5 V. From Figure 3, we see that the solid-state DSSC has not only a lower reference energy, E_r, but also a steeper slope of the $V_{oc}(T)$ relationship. This fact implies that the amount of recombination in the solid-state DSSC is larger than that of the electrolyte cell.

The difference in recombination between the two types of cells results from a basic difference in the recombination mechanism. In the electrolyte DSSC, two oxidized I^- ions form with an additional I^- the triiodide molecule, I_3^- ($2I + I^- \rightarrow I_3^-$). The electron injected into the TiO_2 is not attracted by an overall negatively charged particle, resulting in very low capture cross section for the recombination process.[16] Furthermore, recombination in the electrolyte DSSC is a *two-electron* process according to $2e^- + I_3^- \rightarrow 3I^-$. Such a two-electron process is much more improbable than recombination of a single electron. An additional reason for the low recombination in the electrolyte DSSC is provided by the dipole barrier at the TiO_2 surface (see section II), which hinders the injected electrons from recombining with the I_3^- ions in the electrolyte.

In contrast, in the case of the solid-state hole conductor, the electron leaves back a positive hole, which serves as an attractive partner for recombination. Here recombination is a single-electron process and therefore more probable to happen. By adding lithium salt to the hole conductor, we try to copy the dipole barrier effect at the TiO_2 surface in the electrolyte DSSC. The V_{oc} data above are all measured on solid-state DSSCs containing lithium salt. However, an improvement to the values of the electrolyte DSSC cannot be obtained.

For further investigation, electrolyte and solid-state DSSCs are prepared with and without dye. Because there is almost no current flow without dye (because of no light absorption), only dark *IV* curves are analyzed. According to ref 14, the exited state of the dye is about 0.25 eV above the conduction band edge, E_c, of TiO_2 and could serve as a barrier in dark current transport. Figure 4 demonstrates no difference for the two curves of a solid-state DSSC with and without dye. Saturation current density (J_0), ideality (n_{id}), and series resistance (R_s) in both cases show similar values of $J_0 \approx 10^{-10}$ A cm^{-2}, $n_{id} \approx 1.5$, and $R_s \approx 15\ \Omega$ cm^2. Thus, recombination is independent of the presence of dye at the TiO_2 surface, located between TiO_2 and the electrolyte/hole conductor. This conclusion is compatible with earlier work[34,35] in which it was shown that TiO_2/EL devices without dye display reasonable diode characteristics.

ac Characterization. This section investigates the impedance data of electrolyte DSSC and solid-state DSSC. The impedance, Z, is defined as complex resistance depending on the angular frequency, $\omega = 2\pi f$, of the applied ac voltage as $Z(\omega) = V(\omega)/I(\omega)$ with the frequency-dependent voltage, $V(\omega)$, and current, $I(\omega)$. The data points are weighted using the method suggested in ref 36, which accounts for the measurement with frequency response analyzers. In the following, we concentrate on the device impedance under moderate applied forward voltage bias, that is, in a range relevant for the working conditions of the device.

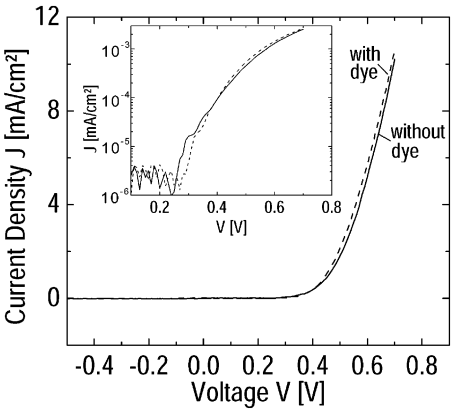

Figure 4. Comparison of dark current−voltage characteristics of solid-state DSSC with and without dye. The presence/nonpresence of the dye has no influence on the dark current either on the linear or on the semilogarithmic scale (see inset).

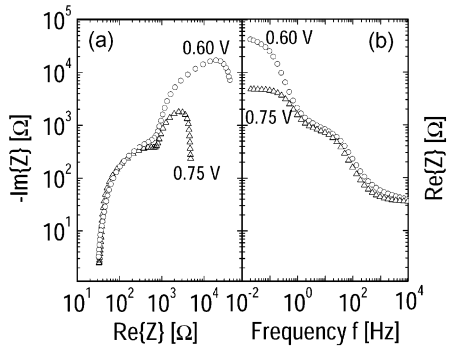

Figure 5. Representations of the frequency-dependent impedance of an electrolyte DSSC measured at $V = 600$ and 750 mV bias in the dark; (a) imaginary, Im(Z), vs real part, Re(Z), of the impedance (Cole−Cole plot); (b) real part, Re(Z), vs frequency, f.

Figure 5 shows two different representations of the frequency-dependent impedance of an electrolyte DSSC (open circles) measured at forward dc bias voltages, $V = 600$ and 750 mV, in the dark. Figure 5a plots the negative imaginary part, $-\mathrm{Im}(Z)$, vs the real part, Re(Z), of the impedance (Cole−Cole plot), and Figure 5b plots Re(Z) vs frequency, f.

The device admittance, $Y(\omega)$, is connected to the impedance data according to $Y(\omega) = 1/Z(\omega)$.[37] From the real part of the admittance, Re(Y), we extract the conductivity, $G(\omega)$; from the imaginary part, Im(Y), we extract the capacitance, $C(\omega)$, of the device. Both, $C(\omega)$ and $G(\omega)$ saturate for low frequencies, $f <$ 100 mHz. To get information about the charge carrier transport, we will restrict ourselves to the analysis of the low-frequency values, C_{lf} and G_{lf}.

Figure 6 shows the low-frequency capacitance, C_{lf}, and the low-frequency conductance, G_{lf}, at 20 mHz of an electrolyte DSSC biased with voltages $V = 0$ V up to $V = 0.75$ V in the dark. Note that in ref 38 we obtain the same capacitance and conductivity values by fitting the impedance data with an equivalent circuit consisting of two parallel circuits of a constant phase element, CPE, and a resistance, R. The capacitance values, C_{lf}, in ref 38 were derived from the capacitive part of the CPE, and both C_{lf} and G_{lf} were taken from the subcircuit with the larger time constant.

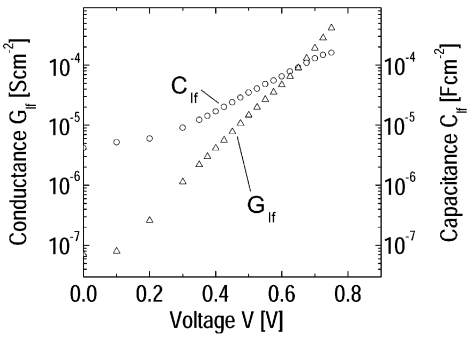

Figure 6. Low-frequency capacitance, C_{lf}, and low-frequency conductance, G_{lf}, versus applied bias voltage, V, for a cell with liquid electrolyte. For $V > 0.3$ V, an exponential increase of both measurements is observed.

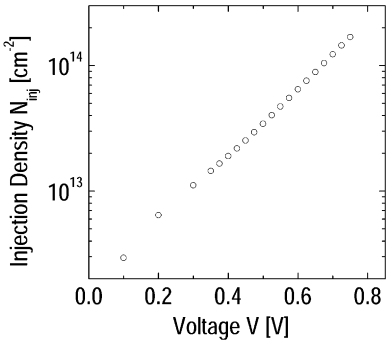

Figure 7. Plot of the injection density, N_{inj}, determined from integration of the low-frequency values of capacitance versus applied potential for a electrolyte DSSC in the dark.

Figure 6 shows exponential increase of both low-frequency admittance values, C_{lf} and G_{lf}. In the following, we assume that in the voltage regime $0.3 \leq V \leq 1.0$ V the device admittance is dominated by the diffusion admittance of electrons in the TiO_2−electrode similarly to the diffusion admittance in classical pn-diodes.[39−41] For those diodes, the exponential increase of diffusion admittance values C_{lf} and G_{lf} is described by the expanded expressions of eqs A2 and A3 in the Appendix. Note that for classical pn-junctions that are dominated by diffusion and recombination the ideality factor, n_{id}, in the diode law should be unity whereas the present devices have $n_{id} \approx 1.4-1.5$. So far, the following calculations must be considered as tentative approaches.

The total amount, N_{inj}, of electrons injected per unit area into the TiO_2 with thickness d_T at a given voltage is given by (see Appendix)

$$N_{inj} = \int_0^{d_T} n(x,V)\, dx \tag{7}$$

Figure 7 shows a plot of the injection density, N_{inj}, versus applied potential, V. At the highest voltage of $V = 0.75$ V, which corresponds approximately to the open-circuit voltage, V_{oc}, of the solar cell, we calculate a injection density of $N_{inj} \approx 1.7 \times 10^{14}$ cm^{-2}. Starting from the measured injected charge, N_{inj}, we calculate the induced voltage drop, ΔV_{if} over the TiO_2−electrolyte interface. Here, we consider two possible situations: either the injected charges are trapped at the surface of the TiO_2 grains, or they are uniformly distributed within the grain. In the first case, $\Delta V_{if} = qN_{inj}/C_{HL}$ where

$$C_{HL} = \frac{\epsilon_{HL}\epsilon_0}{x_{HL}} \frac{d_T}{2gp} \tag{8}$$

is the capacitance of the Helmholtz layer (HL). The symbol x_{HL} denotes the average thickness of the HL, and ϵ_{HL} is the relative dielectric constant of the electrolyte inside the HL, whereas ϵ_0 is the dielectric constant in a vacuum. Using the length, d_T, of a TiO_2 column ($d_T = 4\ \mu$m), its diameter ($g = 20$ nm), a porosity ($p = 0.5$),[28] $\epsilon_{HL} = 5$, and $x_{HL} = 0.5$ nm, we obtain $C_{HL} \approx 1.8 \times 10^{-3}$ F cm^{-2}. Note that the factor $r = d_T/(2gp)$ in eq 8 is the increase in surface area due to the geometry of the electrode, which is $r = 200$ for the assumed column geometry with $N_{inj} \approx 1.7 \times 10^{14}$ cm^{-2}; the voltage drop V_2 over the TiO_2−electrolyte interface is therefore approximately 15 mV. Thus, V_2 is only a small part of the externally applied voltage of 750 mV in our example.

If the injected electrons were uniformly distributed over the grain volume, they would induce a band bending within the TiO_2 nanograins. Considering again a film thickness d_T of 4 μm and a porosity of 0.5,[28] we estimate an electron concentration $n_e = N_{inj}/0.5d_T$ of $n_e \approx 8.5 \times 10^{17}$ cm^{-3}. By using the expression for the width of a space charge region for an abrupt one-sided semiconductor junction,[42] we estimate the voltage drop due to the band bending, V_{bb}, across the diameter of a single TiO_2 grain

$$V_{bb} = \frac{n_e q}{8\epsilon_0\epsilon_r} g^2 \tag{9}$$

where we use $\epsilon_r = 9$[43] as the relative dielectric constant. The maximum width of a space charge region caused by the additional charge density due to injection is half of the grain diameter, $g \approx 20$ nm. From eq 9, we find $V_{bb} \approx 85$ mV. Note that the two-dimensional numerical simulations of Ferber and Luther[21] obtain a difference between the electrostatic potential in the electrolyte and that in the TiO_2 of approximately 30 mV under illumination at open-circuit conditions. The numerically simulated value of 30 mV is just between the 15 mV and the 85 mV estimated above as the two limiting cases for the voltage drop V_2.

However, under none of the above assumptions, the voltage drop V_2 is in the range of the external bias voltage. Therefore in the voltage regime $0.3 < V < 0.75$ V, the diffusion capacitance, C_{diff}, of injected electrons is the dominant capacitive element in the device. Only at higher voltage bias when the exponentially increasing diffusion capacitance, C_{diff}, becomes comparable to C_{HL}, the measured capacitance saturates at C_{HL}, which was in fact observed by Zaban et al. (Figure 2 in ref 18 at voltages $V > 1$ V). It is in the same voltage range where we observe the saturation of the low-frequency capacitance of our devices. In turn, under moderate forward bias, that is, in the voltage range of V_{oc}, the device capacitance is dominated by diffusion and the voltage drop over the TiO_2−electrolyte interface is negligible.

For the solid-state DSSC, we observe a quite different behavior compared to the admittance of cells with liquid electrolyte. Figure 8 shows the experimental data for C_{lf} and G_{lf} measured at 50 mHz. The main difference compared to the data in Figure 6 is the occurrence of a negative capacitance (i.e., inductance) at voltages $V > 0.3$ V, while the conductance G_{lf} shows an exponential increase in a voltage range $0.15 \leq V \leq 0.5$ V. In classical pn-junctions, such inductive behavior is well-known as resulting from series resistance modulation by injection of minority carriers.[10] In our situation, electrons injected into the TiO_2 modulate the number of holes in the hole conductor and thus reduce the resistance within the pores. The time delay between electron injection and the modulation of

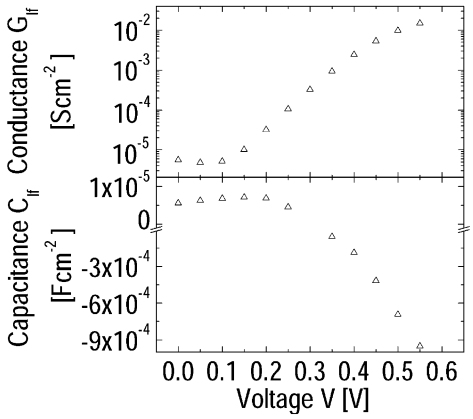

Figure 8. Capacitance, C_{lf}, and conductance, G_{lf}, measured at 50 mHz for a solid-state DSSC under forward bias, V. For voltages > 0.3 V, the capacitance, C_{lf}, shows negative values, which unveils an inductive behavior. The observed inductance can be explained by electrons injected into the TiO_2, which modulate the number of holes in the surrounding HC.

the hole concentration then leads to the observed inductive behavior. As described by Misawa,[10] such a modulation effect is expected to occur as soon as the density of injected electrons approaches about 60% of the density of holes. From the fact that inductive effects show up for voltages as low as 0.3 V, we conclude that not only the overall conductivity of the hole conductor but also its effective hole density is low. Taking the injected electron density in the TiO_2 from the liquid DSSC at $V = 0.3$ V, we estimate the equilibrium hole concentration, p_0, in the HC to be on the order of $p_0 = 10^{17}$ cm^{-3}.

V. Discussion

In this paper, we have used an analogy, especially for the ac transport properties, between classical solid-state pn-(heterojunction) and DSSCs. In view of the ongoing discussion on "the origin of the photovoltage in DSSCs",[16,19,21,22] we have to comment on the implications underlying such an analogy. As mentioned before, we distinguish between that analogy and the more specific question on the magnitude of the built-in voltage.

Diffusion Capacitance. The occurrence of a diffusion capacitance in DSSCs has two implications: (i) The injected electrons in the TiO_2 of the electrolyte cell are well screened by the surrounding electrolyte similarly as the charge of injected minority carriers in the base region of a pn-junction is screened by the majority carriers. Therefore, we can use the time-dependent diffusion equation without contribution from any electrical field to compute the diffusion capacitance of the electrolyte cell. If a pn-junction diode approaches high-injection conditions, the minority carriers modulate the density of majorities to maintain local charge neutrality, which gives rise to inductive behavior of the junction impedance.[10] In this picture, the observation of a negative reactance in the solid-state cell implies that the electrons in the TiO_2 have sufficient electrostatic interaction with the holes in the HC to enable such a conductivity modulation. Obviously, the charge neutrality condition used for classical pn-junctions to model the junction impedance[10] holds in the DSSC only in a spatial average over the TiO_2 column and the surrounding HC because in the DSSC positive and negative charges are situated in different media. However, the distance between the charges in the nanoscale mixture of TiO_2 and HC is only few nanometers, that is, small compared to the thickness d_T of the active region of the device. Therefore, we believe that the Misawa model[10] is a reasonable first-order approach for what is observed in the solid-state DSSC. (ii) Because the diffusion capacitance (as well as the dark current) of the electrolyte DSSC increases exponentially with applied voltage, the number of the electrons injected into the TiO_2 (and their subsequent recombination with the I_3^- ions) must be controlled by some rectifying junction.

Photovoltage and Built-In Voltage. Obviously, statement ii in the preceding section leads us into the center of the ongoing discussion on the "kinetic model"[16-18] and the "junction model"[19] for DSSCs. Here, our position is rather relaxed, and we do not flinch from taking out elements of both approaches.

Any type of solar cell needs a capacitive element that is able to translate electrochemical potential differences into shifts of the electrical potential and, thereby, enables measurement of a photovoltage at the outer electrodes of the device. From our experiments, we conclude that in the DSSC this capacitive element is the junction between SnO_2/F−TiO_2 where the charges necessary to make a built-in voltage are borrowed from the electrolyte or the HC. In so far, we follow the "junction model". There is, however, no physical law that implies that the open-circuit voltage of a solar cell cannot exceed the dark built-in voltage of its junction. Therefore, we follow the "kinetic model" for what concerns the fundamental limitations of the *open-circuit voltage*. However, a complete model for DSSCs, that is, a model that quantitatively describes the diode characteristics including ideality factors, $n_{id} > 1$, should cover both aspects, kinetic limitations and carrier injection/extraction by the junction.

Estimate of Fill Factor Losses. The band diagram in Figure 2c, for what concerns the electron flow from the TiO_2 into the SnO_2/F substrate, is a Schottky contact with barrier height $\Phi_b = \Delta E_c = \chi_{SnO_2} - \chi_{TiO_2}$. Let us assume that the current through the field region of the junction is dominated by thermal emission of electrons from the TiO_2 into the SnO_2/F according to[44]

$$J = A^*T^2 \exp(-\Phi_b/(kT))[1 - \exp(q\Delta V_l/(kT))] \quad (10)$$

A^* being the Richardson constant of TiO_2 and the loss voltage, ΔV_l, being as defined in Figure 2c. For the sake of current continuity, the current density J has to be equalized to that of the main, photovoltaic-active diode

$$J = J_0[\exp(qV/(n_{id}kT)) - 1] - J_{sc} \quad (11)$$

Solving eqs 10 and 11 for the voltages ΔV_l and V, respectively, allows us to compute the externally measured voltage, $V_{ext} = V - \Delta V_l$, for any current density J with $A^*T^2 \exp(-\Phi_b/(kT)) > J > -J_{sc} - J_0$. Figure 9 shows three *IV* curves computed using $J_0 = 1.6 \times 10^{-7}$ mA cm^{-2}, $J_{sc} = 40$ mA cm^{-2}, and $n_{id} = 1.5$ for the main diode, as well as $A^* = 670$ A cm^{-2} K^{-2}, and barrier heights $\Phi_b = 0.5$, 0.6, and 0.65 eV for the secondary diode that builds up at the TiO_2−SnO_2/F contact. Note that the current densities, J_0 and J_{sc}, in the above example were both chosen four times higher than the values that are typically measured in an EL DSSC because the electron flow across the interface concentrates to those places where the TiO_2 comes into contact with the SnO_2/F. The diode ideality factor, $n_{id} = 1.5$, corresponds to what we typically measure in our EL DSSCs.

At open circuit, the current density J is zero; hence, $V = V_{oc}$ from eq 11 and $\Delta V_l = 0$ from eq 10. Thus, the external voltage equals the open-circuit voltage, that is, $V_{ext} = V_{oc}$, and all *IV* curves in Figure 9 cross the voltage axis at the same open-circuit voltage, V_{oc}, independently of Φ_b. Thus, the experimental finding that V_{oc} in El DSSCs is independent of the work function of the front electrode[22] resulting in different values for $\Phi_b = \Delta E_c$ is compatible with our simple approach.

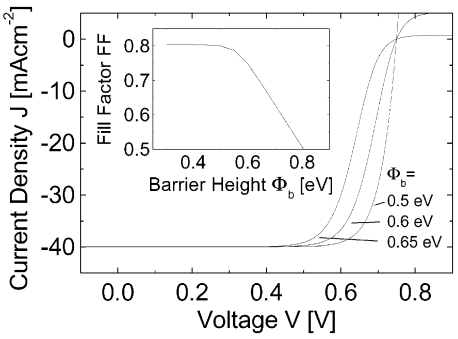

Figure 9. Current density vs voltage curves computed by equalizing eqs 10 and 11 using $J_0 = 1.6 \times 10^{-7}$ mA cm^{-2}, $J_{sc} = 40$ mA cm^{-2}, and $n_{id} = 1.5$ for the main diode, as well as $A^* = 670$ mA cm^{-2} K^{-2} and barrier heights $\Phi_b = 0.5$, 0.6, and 0.65 eV for the secondary diode at the TiO_2-SnO_2/F contact. The current densities J_0 and J_{sc} were chosen four times higher than the values typically measured in an EL DSSC because the current is concentrated to places where the TiO_2 comes into contact with the SnO_2/F. The open-circuit voltage, $V_{oc} = 0.75$ V, is independent of Φ_b and, consequently, independent from the initial built-in voltage, V_{bi}^0. However, as shown in the inset, the fill factor is independent from the barrier height, $\Phi_b = \Delta E_c$, only up to $\Phi_b \approx 0.6$ V.

However, the fill factor of the *IV* curves starts to degrade if $\Phi_b > 0.6$ eV as shown in the inset of Figure 9. Considering

$$\Delta E_c + qV_{bi}^0 = E_c - E_{redox} \tag{12}$$

from Figure 2a and $E_c - E_{redox} \approx 1.2$ eV from our experimental data, we estimate a *lower limit* of around 0.6 V for the built-in voltage, V_{bi}^0, that is compatible with a good fill factor. Notably, this value is just in the middle of the presumptions of refs 16 and 19 and is also within the range for V_{bi}^0 given by Ferber and Luther.[21]

VI. Conclusions

Both DSSCs, those with a liquid electrolyte and those with a solid-state hole conductor, exhibit a linear dependence of the open-circuit voltage, V_{oc}, on temperature, T. The (extrapolated) reference energy, $E_r = qV_{oc}$ ($T = 0$ K), of the electrolyte cell is $E_r^{el} \approx 1.2$ eV, whereas for the solid-state cell, we find $E_r^{ss} \approx 1.0$ eV. However, this difference, $\Delta E_r = E_r^{el} - E_r^{ss}$, of around 0.2 eV cannot entirely explain the low V_{oc} of the solid-state cell, which (with typically $V_{oc} = 450$ mV) is more than 300 mV below the V_{oc} of the electrolyte reference cells. Thus, another 100−200 mV V_{oc} loss of the solid-state cell with respect to the electrolyte reference must be due to the high recombination probability of photogenerated electrons from the TiO_2 into the hole conductor.

Another peculiarity of solid-state DSSC devices is unveiled by impedance analysis. Electrolyte DSSCs exhibit an exponential increase of the low-frequency device capacitance due to the diffusion of electrons along the TiO_2 network. In contrast, the solid-state DSSCs show a *negative reactance*. In those devices, the junction impedance exhibits inductive behavior as soon as injection into the TiO_2 approaches high-injection conditions, that is, as soon as the number of injected electrons comes close to the number of holes in the HC. The onset of inductive behavior in our solid-state DSSC is already at voltages as low as 0.3 V. Therefore, we conclude that the doping of the HC is too low to maintain proper working conditions of the device. As a consequence, the basic problems that we need to overcome for constructing higher efficiency solid-state DSSCs are (i) the high recombination rate at the TiO_2/HC interface and (ii) the low conductivity of the hole conductor itself. Regardless of their differences, both devices, the EL and the solid-state DSSC, are qualitatively and, to a certain extent, quantitatively described by their analogy to pn-(hetero)junctions.

Acknowledgment. The authors gratefully acknowledge the support by Sony International (Europe). We thank G. Nelles, T. Miteva, and A. Yasuda for collaboration and discussions, as well as C. Gemmer for a critical reading of the manuscript.

Appendix

Diffusion Admittance. According to Shockley,[9] the diffusion admittance of minority carriers for classical pn junctions ($V > 3kT/q$) is given by

$$Y_{diff} = \frac{qn_j D_e}{L_{De}^*}\frac{q}{kT}\tanh\frac{d_T}{L_{De}^*} \tag{A1}$$

From eq A1, we expand the diffusion admittance, Y_{diff}, for $\omega\tau_e \ll 1$ as $Y_{diff} = G_{diff}^{lf} + i\omega C_{diff}^{lf}$ with

$$G_{diff}^{lf} = \frac{qn_j D_e}{L_{De}}\frac{q}{kT}\tanh\frac{d_T}{L_{De}} \tag{A2}$$

and

$$C_{diff}^{lf} = \frac{qn_j L_{De}}{2}\frac{q}{kT}\left\{\tanh\frac{d_T}{L_{De}} + \frac{\dfrac{d_T}{L_{De}}}{\cosh^2\dfrac{d_T}{L_{De}}}\right\} \tag{A3}$$

Injected Charge. Integrating the solution of the diffusion equation, $n(x,V)$, which we obtain from the general solution[45] by neglecting recombination at the end of the TiO_2 column at d_T, yields

$$N_{inj} = n_j L_{De}\tanh\frac{d_T}{L_{De}} \tag{A4}$$

Comparing eq A3 with eq A4 yields

$$C_{diff}^{lf} = \frac{d(qN_{inj})}{dV}\frac{1}{2}\frac{\tanh\dfrac{d_T}{L_{De}} + \dfrac{d_T}{L_{De}}\cosh^{-2}\dfrac{d_T}{L_{De}}}{\tanh\dfrac{d_T}{L_{De}}}$$

$$= \frac{d(qN_{inj})}{dV}\frac{1}{2}\left(1 + \frac{\dfrac{d_T}{L_{De}}}{\cosh\dfrac{d_T}{L_{De}}\sinh\dfrac{d_T}{L_{De}}}\right) = \frac{d(qN_{inj})}{dV}\alpha \tag{A5}$$

with $0.5 \le \alpha \le 1$. Thus, within an error on the order of unity, eq A5 allows calculation of the injected charge, $qN_{inj} \approx \int_0^V C_{lf}\,dV'$.

References and Notes

(1) Vlachopoulos, N.; Liska, P.; Augustinsky, J.; Graetzel, M. *J. Am. Chem. Soc.* **1988**, *110*, 1216.
(2) O'Regan, B.; Graetzel, M. *Nature* **1991**, *353*, 737.
(3) Nazeeruddin, M. K.; Kay, A.; Rodicio, I.; Humphry-Baker, R.; Müller, E.; Liska, P.; Vlachopoulus, N.; Grätzel, M. *J. Am. Chem. Soc.* **1993**, *115*, 6382.

(4) Nogueira, A. F.; De Paoli, M. A. *Sol. Energy Mater. Sol. Cells* **2000**, *61*, 135.
(5) Bach, U.; Lupo, D.; Compte, P.; Moser J. E.; Weissörtel, F.; Salbeck, J.; Spreitzer, H.; Grätzel, M. *Nature* **1998**, *359*, 583.
(6) Hagen, J.; Schaffrath, W.; Otschik, P.; Fink, R.; Bacher, A.; Schmidt, H. W.; Haarer, D. *Synth. Met.* **1997**, *89*, 215.
(7) Tennakone, K.; Kumara, G. R. R. A.; Kumarasinghe, A. R.; Wijayantha, K. G. U.; Sirimanne, P. M. *Semicond. Sci. Technol.* **1995**, *10*, 1689.
(8) Gregg, A. G.; Pichot, F.; Ferrere, S.; Fields, C. L. *J. Phys. Chem. B* **2001**, *105*, 1422.
(9) Shockley, W. *Bell Syst. Tech. J.* **1949**, *28*, 435.
(10) Misawa, T. *J. Phys. Soc. Jpn.* **1959**, *12*, 882.
(11) Tachibana, Y.; Moser, J. E.; Graetzel, M.; Zhang, J. Z. *J. Phys. Chem. B* **1997**, *100*, 20056.
(12) Cherepy, N. J.; Smestad, G. P.; Graetzel, M.; Zhang, J. Z. *J. Phys. Chem. B* **1997**, *101*, 9342.
(13) Hilgendorff, M.; Sundström, V. *J. Phys. Chem. B* **1998**, *102*, 10505.
(14) Hagfeldt, A.; Grätzel, M. *Acc. Chem. Res.* **2000**, *33*, 269.
(15) O'Regan, B.; Moser, J.; Anderson, M.; Grätzel, M. *J. Phys. Chem.* **1990**, *94*, 8720.
(16) Cahen, D.; Hodes, G. J.; Graetzel, M.; Guillemoles, J.-F., Riess, I. *J. Phys. Chem. B* **2000**, *104*, 2053.
(17) Zaban, A.; Ferrere, S.; Gregg, B. *J. Phys. Chem. B* **1998**, *102*, 452.
(18) Zaban, A.; Ferrere, S.; Gregg, B. *J. Phys. Chem. B* **1997**, *101*, 7985.
(19) Schwarzburg, K.; Willig, F. *J. Phys. Chem. B* **1999**, *103*, 5743.
(20) Bisquert, J.; Garcia-Belmonte, G.; Fabregat-Santiago, F. *J. Solid State Electrochem.* **1999**, *3*, 337.
(21) Ferber, J.; Luther, J. *J. Phys. Chem. B* **2001**, *105*, 4895.
(22) Pichot, F.; Gregg, B. *J. Phys. Chem. B* **2000**, *104*, 6.
(23) Gerischer, H. In *Physical Chemistry. an Advanced Treatise*; Eyring, H., Ed.; Academic Press: New York, London, 1970; Vol. 9, p 463.
(24) Rosenbluth, M. L.; Lewis, N. S. *J. Phys. Chem.* **1989**, *93*, 3735.
(25) Pleskov, Yu. V.; Gurevich, Yu. Ya. *Semiconductor Photoelectrochemistry*; Consultants Bureau: New York, London, 1986; pp 135−138.
(26) Morrison, S. R. *Electrochemistry at Semiconductor and Oxidized Metal Electrodes*; Plenum Press: New York, London, 1980; p 98.
(27) Equation 2b is obtained by reorganizing the interface recombination equation in Bube, R. H. *Photoelectronic Properties of Semiconductors*; Cambridge University Press: Cambridge, U.K. 1992; p 257.
(28) Hagfeldt, A.; Grätzel, M. *Chem. Rev.* **1995**, *95*, 49.
(29) Gutman, F.; Lyons, L. E. *Organic Semiconductors*; John Wiley & Sons: New York, 1967; p 61.
(30) Kavan, L.; Grätzel, M. *Electrochim. Acta* **1995**, *40* (5), 643.
(31) Salbeck, J.; Weissörtel, F.; Bauer, *J. Macromol. Symp.* **1997**, *125*, 121.
(32) Salbeck, J.; Yu, N.; Bauer, J.; Weissörtel, F.; Bestgen, H. *Synth. Met.* **1997**, *91*, 209.
(33) Nozik, A. J.; Memming, R. *J. Phys. Chem.* **1996**, *100*, 13061.
(34) Shiga, A.; Tsujiko, A.; Ide, T.; Yae, S.; Nakato, Y. *J. Phys. Chem. B* **1998**, *102*, 6049.
(35) Subramanian, V.; Wolf, E.; Kamat, P. V. *J. Phys. Chem. B* **2001**, *105*, 11439.
(36) Spinolo, G.; Chiodelli, G.; Magistris, A.; Tamburini, U. *J. Electrochem. Soc.* **1988**, *135*, 1419.
(37) Macdonald, J. R. *Impedance Spectroscopy*; John Wiley & Sons: New York, 1987; p 7.
(38) Kron, G.; Egerter, T.; Nelles, G.; Yasuda, A.; Werner, J. H.; Rau, U. *Thin Solid Films* **2002**, *403*−*404*, 242.
(39) Sze, S. M. *Physics of Semiconductor Devices*, 2nd ed.; J. Wiley & Sons: New York, 1986; p 94.
(40) Neudeck, G. W. *The PN Junction Diode*, 2nd ed.; Addison-Wesley: Reading, MA, 1989; p 105.
(41) Möschwitzer, A.; Lunze, K. In *Halbleiterelektronik*; Hüthig, A., Ed.; Verlag: Heidelberg, 1980; p 178 ff.
(42) Seto, J. Y. W. *J. Appl. Phys.* **1975**, *46* (12), 5247.
(43) Dittrich, Th.; Weidmann J.; Koch F.; Uhlendorf I.; Lauermann I. *Appl. Phys. Lett.* **1999**, *75*, 3980.
(44) Rhoderick, E. H.; Williams, R. H. *Metal-Semiconductor Contacts*, 2nd ed.; Clarendon Press: Oxford, U.K., 1988; p 15.
(45) Tyagi, M. S. *Introduction to Semiconductors Materials and Devices*; J. Wiley & Sons: New York, 1991; p 189.